Journal of Applied Physics

Effect of disorder and vacancy defects on electrical transport properties of Co_2MnGa thin films grown by magnetron sputtering

Cite as: J. Appl. Phys. **130**, 225301 (2021); https://doi.org/10.1063/5.0071807
Submitted: 16 September 2021 • Accepted: 22 November 2021 • Published Online: 10 December 2021

A. Miyashita, M. Maekawa, C. Suzuki, et al.

Journal of Applied Physics ARTICLE scitation.org/journal/jap

Effect of disorder and vacancy defects on electrical transport properties of Co_2MnGa thin films grown by magnetron sputtering

Cite as: J. Appl. Phys. **130**, 225301 (2021); doi: 10.1063/5.0071807
Submitted: 16 September 2021 · Accepted: 22 November 2021 ·
Published Online: 10 December 2021

A. Miyashita,[1] M. Maekawa,[1] C. Suzuki,[1] S. Yamamoto,[1] A. Kawasuso,[1,a)] J. Wang,[2,3] T. Seki,[2,3] R. Y. Umetsu,[2,3,4] and K. Takanashi[2,3,4]

AFFILIATIONS

[1]National Institutes for Quantum and Radiological Science and Technology, 1233 Watanuki, Takasaki, Gunma 370-1292, Japan
[2]Institute for Materials Research, Tohoku University, 2-1-1, Katahira, Aoba-ku, Sendai 980-8577, Japan
[3]Center for Spintronics Research Network, Tohoku University, 2-1-1, Katahira, Aoba-ku, Sendai 980-8577, Japan
[4]Center for Science and Innovation in Spintronics, Core Research Cluster, Tohoku University, 2-1-1, Katahira, Aoba-ku, Sendai 980-8577, Japan

[a)]**Author to whom correspondence should be addressed:** kawasuso.atsuo@qst.go.jp

ABSTRACT

Co_2MnGa is known as a Weyl semimetal exhibiting giant anomalous Hall and Nernst effects. However, the performance of Co_2MnGa thin films grown on MgO(001) by the magnetron sputtering method is somewhat lower than that of the bulk crystals. Here, we attempted to improve the electrical transport properties by post-growth annealing at temperatures from 573 to 773 K. X-ray diffraction analysis indicated that the degree of long-range order changed from $A2$ to $B2$ plus $L2_1$ upon annealing at 673 K or above. Positron annihilation spectroscopy revealed the presence of high-density ($\gtrsim$100 ppm) divacancies, which were absent in the bulk crystal, and their partial improvement near the Co_2MnGa/MgO interface on annealing at 673 K or above. Accompanying these structural changes, the longitudinal and anomalous Hall conductivities increased considerably and the anomalous Hall angle reached a maximum value of 11.8%. These findings imply that the post-growth annealing improved the electrical transport properties of Co_2MnGa films through the development of long-range crystal order and reduction of divacancies. However, the electrical performance achieved by thermal annealing was still insufficient in comparison with the bulk crystals, and hence for further improvement, alternative approaches may need to be considered.

I. INTRODUCTION

Some X_2YZ-type full Heusler alloys are predicted to be ferromagnetic Weyl semimetals.[1,2] In fact, Weyl semimetallicity has been confirmed for Co_2MnGa bulk single crystals through the observation of linear band dispersions by photoemission spectroscopy.[3] Furthermore, the giant anomalous Hall and Nernst effects observed for Co_2MnGa have been attributed to the intrinsic mechanism owing to the large Berry curvature associated with this compound.[3–5] In addition, photoemission spectroscopy results have demonstrated the existence of the characteristic Weyl semimetal band structure for Co_2MnGa thin films deposited on MgO(001) substrates by magnetron sputtering.[6]

However, the anomalous Hall conductivities observed for Co_2MnGa thin films are generally lower than those for the bulk single crystals.[6–8] Moreover, the sign of the thermoelectric conductivity is not necessarily consistent with that predicted from theory.[6] On the other hand, the anomalous Hall conductivity of Co_2MnGa thin films is found to improve with the development of ordered structures at relatively high deposition temperatures.[7,8] Nevertheless, the anomalous Hall conductivity remains far from ideal.

The perfect crystal structure of X_2YZ-type full Heusler alloys is denoted as $L2_1$. Atomic swaps may occur between X and Y, X and Z, Y and Z, or X, Y, and Z, resulting in disordered structures. The Y–Z and X–Y–Z-disordered structures are referred to as $B2$

and $A2$, respectively. Under non-stoichiometric conditions, excess antisite defects may also be introduced depending on the precise composition. In previous studies, the electrical transport properties of Co_2MnSi were proposed to be influenced by Co/Mn disorder or excess Co/Mn antisite defects.[9] Theoretical studies have suggested that disorder and excess antisite defects degrade the half-metallicity and electrical performance of Co_2-based Heusler alloys.[10–16] The inclusion of a large amount of vacancies was also found experimentally for Co_2MnZ (Z = Si, Ge, Sn).[17] Theoretical studies again suggested that vacancies also lead to the deterioration of the half-metallicity and electrical transport properties of Co_2-based Heusler alloys.[13,16,18,19] The crystal disorder and defects are thus important issues in Co_2-based Heusler alloys.

In this study, we examined the crystallinity of Co_2MnGa thin films prepared using various post-growth annealing temperatures by transmission electron microscopy (TEM) and x-ray diffraction (XRD) analysis. Furthermore, to inspect the inclusion of vacancy defects, which have been overlooked to date, positron annihilation spectroscopy[20,21] was employed. The results indicate the inclusion of high-density divacancies (more than at least 100 ppm) during the epitaxial growth of Co_2MnGa, alongside the development of an ordered structure. The influences of disorder and divacancies on the electrical properties of Co_2MnGa thin films are also discussed.

II. METHODS

The samples used in the present work were Co_2MnGa films with a target thickness of 75 nm grown on MgO(001) substrates by the magnetron sputtering method at room temperature.[7] To prevent oxidation in air, AlO_x cap layers with a thickness of approximately 2 nm were deposited on the films. The films were then subjected to *in situ* annealing at $T_A = 573$, 673, or 773 K for 3 h under vacuum. Finally, the samples were examined by TEM, energy-dispersive x-ray (EDX) analysis, XRD analysis, magnetization (M–H) measurements at room temperature, and Hall effect measurements at 10–296 K.

Positron annihilation measurements based on the Doppler broadening of annihilation radiation (DBAR) method were conducted using a variable-energy slow positron beam generated from a ^{22}NaCl source. Vacancy defects were characterized by the so-called S parameter, which is defined as the peak area intensity in the DBAR spectrum. It represents the contribution of valence electrons to the annihilation with positrons.[20,21] At vacancies, the annihilation probability between positrons and valence electrons increases and hence the S parameter is relatively higher than that in the bulk region. The S parameter also increases and tends to become saturated as the vacancy concentration increases from a few ppm to more than approximately 100 ppm. In the positron annihilation measurements, an $L2_1$-ordered Co_2MnGa bulk single crystal grown by the Bridgman method[22–24] and a $B2$-ordered Co_2MnAl polycrystal prepared by arc melting followed by heat treatment at 1473 K for 20 h were used as references.

To identify the vacancy defects observed in the positron annihilation measurements, density functional theory (DFT) calculations were conducted using the ABINIT code[25] with the projector augmented-wave method[26] within the generalized gradient approximation.[27] The system was a $2 \times 2 \times 2$ conventional cell composed of 128 atoms with the experimental lattice constants (5.77 Å for Co_2MnGa and 5.75 Å for Co_2MnAl).[28,29] [The $1 \times 1 \times 1$ conventional cell is defined as a cubic cell including eight body-centered cubic (bcc) cells, where Co atoms occupy the corner positions, and Mn and Ga atoms occupy the neighboring body-centered positions. The $2 \times 2 \times 2$ system had enough size in the present calculation.] The valence electron configurations were assumed to be $3s^2 3p^6 3d^8 4s^1$ (Co), $3s^2 3p^6 3d^6 4s^1$ (Mn), $3d^{10} 4s^2 4p^1$ (Ga), and $3s^2 3p^1$ (Al). Positron wave functions were obtained using two-component DFT.[30] The Slater functions[31] were used as core electron wave functions. The Borónski–Nieminen enhancement factor[30] was adopted. Finally, the DBAR spectra were obtained by double integrating the momentum density and convoluting with the Gaussian resolution function having a full width at half maximum of 5.488×10^{-3} m_0c.

III. RESULTS AND DISCUSSION

A. Structural characterization

Figure 1(a) presents TEM images and diffraction patterns obtained for the Co_2MnGa films after annealing. For $T_A = 573$ K, the low-magnification image indicated that the film is composed of columnar crystals oriented to the [001] direction with a typical size of 10–30 nm in the surface-parallel direction. The diffraction pattern exhibited the Debye–Scherrer ring, suggesting that the columnar crystals had different orientations in the surface-parallel direction. On the other hand, the clear lattice fringes observed in the high-magnification image indicated the epitaxial growth of Co_2MnGa in individual columnar crystals. For $T_A = 673$ and 773 K, the low-magnification images indicated the significant suppression of columnar crystals. Furthermore, the diffraction patterns indicated the cubic lattice periodicity instead of the Debye–Scherrer ring. Similarly to $T_A = 573$ K, the high-magnification images exhibited clear lattice fringes, confirming the epitaxial growth of Co_2MnGa. These suggested the coalescence of columnar crystals and consequent development of more homogenous textures at $T_A = 673$ and 773 K. The film thicknesses measured in the TEM observation were 69 nm for the films annealed at 573 and 673 K and 65 nm for the film annealed at 773 K.

Figures 1(b) and 1(c) show the EDX depth profiles and the two-dimensional maps through the films, respectively. Homogeneous distributions of Co, Mn, and Ga were obtained for all samples, irrespective of the annealing temperature. The intensity of Mn was found to be lower for $T_A = 673$ and 773 K. Since in-diffusion and clustering of Mn atoms were not apparently seen, the Mn depletion indicated the sublimation of Mn atoms upon heating due to its high vapor pressure and the vacuum conditions. The average compositions are listed in Table I.

Figures 2(a)–2(c) show the XRD patterns obtained in the out-of-plane (a) and tilted [(b) and (c)] scan modes. The observation of only (h00) reflections (h = 2 and 4) in the out-of-plane scan mode under all annealing conditions further indicated the occurrence of epitaxial growth, in accordance with the TEM analysis described above. The appearance of superlattice reflections, namely, (200) for $T_A = 673$ and 773 K and (111) for $T_A = 773$ K, indicated the development of $B2$- and $L2_1$-ordered structures, respectively. From these XRD data, the degrees of order for the $A2$, $B2$, and $L2_1$ phases were determined using the following

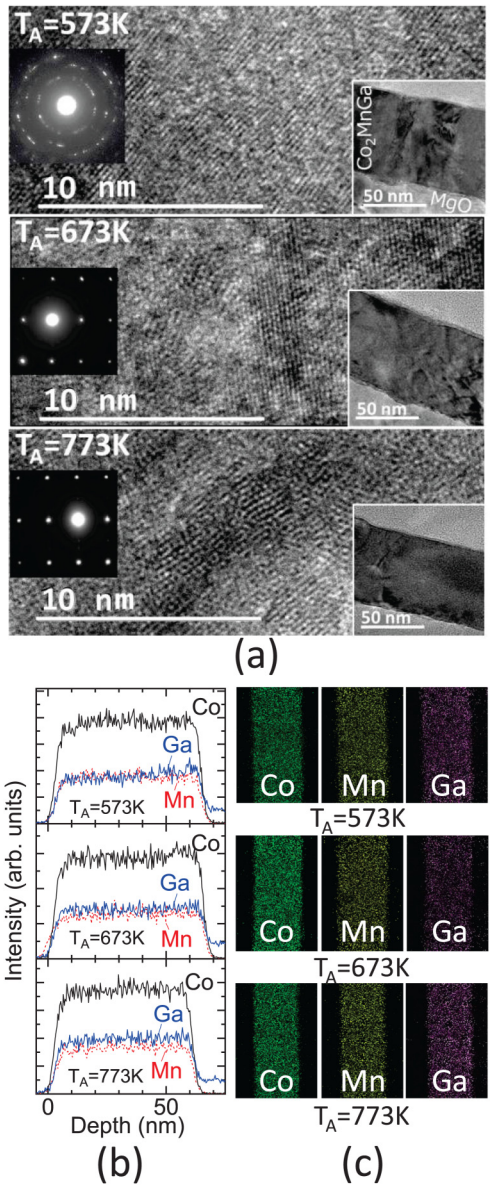

FIG. 1. (a) TEM images and diffraction patterns, (b) EDX depth profiles, and (c) EDX two-dimensional maps obtained for Co_2MnGa films after annealing at 573, 673, and 773 K.

equations:[32]

$$S_{B2} = \sqrt{[I_{200}/I_{400}]_{exp}/[I_{200}/I_{400}]_{cal}}, \quad (1)$$

$$S_{L2_1} = 2\sqrt{[I_{111}/I_{400}]_{exp}/[I_{111}/I_{400}]_{cal}}/(3 - S_{B2}), \quad (2)$$

where I and its subscript denote the peak intensity and the diffraction index, respectively, and exp and cal denote the experimental and calculated intensities, respectively. The obtained degrees of the order are listed in Table I. After annealing at 573 K, only the $A2$ phase (100%) was detected. In contrast, after annealing at 673 K, the fraction of the $B2$ phase dramatically increased (87%). Furthermore, after annealing at 773 K, the $L2_1$ phase (23%) was found to have developed in addition to the $B2$ phase.

B. Positron annihilation measurements

Figure 3 shows the positron annihilation S parameters as functions of the incident positron energy and mean positron implantation depth (calculated with the density of Co_2MnGa) measured for the Co_2MnGa films after annealing. The horizontal axis is divided into three parts, i.e., the AlO_x region below 1 keV, the Co_2MnGa region between approximately 1 and 6 keV, and the MgO region approximately above 6 keV. The AlO_x layers are not clearly visible from these plots, which is presumably attributable to their thinness. The S parameters changed from relatively high values in the Co_2MnGa region to lower values in the MgO region with increasing incident positron energy. (The errors were within the circles.) The S parameters obtained for the bulk Co_2MnGa and Co_2MnAl samples at 15–20 keV are indicated as horizontal lines in Fig. 3(b). As compared to the bulk Co_2MnAl sample, for which the vacancy concentration is under the detection limit, the S parameter for the bulk Co_2MnGa sample was higher, suggesting the inclusion of vacancy defects. The S parameters for the Co_2MnGa films were even greater than that for bulk Co_2MnGa, indicating a larger open-volume size and/or a higher concentration of vacancy defects.

To determine the vacancy species and their concentrations, Fig. 4 shows the DBAR spectra obtained for the Co_2MnGa films and bulk Co_2MnGa with respect to the reference spectrum for bulk Co_2MnAl [$N(p)/N_{ref}(p)$, where $N(p)$ denotes the DBAR spectrum as a function of electron momentum p] together with the theoretical curves for various single vacancies (V_{Co}, V_{Mn}, and V_{Ga}) and nearest-neighbor divacancies ($V_{Co}V_{Mn}$ and $V_{Co}V_{Ga}$). (The experimental error bar tends to increase with increasing electron momentum due to the suppression of counting rate in the high momentum region.) The spectra for the Co_2MnGa film and bulk samples were integrated at 2–4 and 15–20 keV, respectively, for better statistics. It can be seen that the experimental spectrum for the bulk Co_2MnGa sample was comparable to the theoretical curves for single vacancies, suggesting the inclusion of single vacancies in this sample. Furthermore, nearly all of the positrons were trapped by single vacancies, and hence the concentration of single vacancies was more than at least 100 ppm. In contrast, the experimental spectra for the Co_2MnGa films were similar to the calculated curves for divacancies but not to those for single vacancies. We also examined larger vacancy clusters such as quadravacancies [$2\times(V_{Co}V_{Mn})$ and $2\times(V_{Co}V_{Ga})$) and hexavacancies ($2\times(V_{Co}V_{Mn}V_{Ga})$]. However, these larger vacancy clusters did not reproduce the experimental curves. Thus, the Co_2MnGa films contained divacancies as the major positron-trapping centers and their concentration was more than at least 100 ppm.

Returning to Fig. 3, the S parameters below 4 keV exhibited almost no changes up to $T_A = 773$ K, suggesting that the divacancy

TABLE I. Analytical data obtained for the Co_2MnGa films after post-growth annealing at 573, 673, and 773 K.

Anneal temp. (K)	Composition			Structure			Magnetization at RT (μ_B/f.u.)	Transport at 10 K		
	Co (%)	Mn (%)	Ga (%)	*A*2 (%)	*B*2 (%)	$L2_1$ (%)		σ_{xx} (S/cm)	σ_{xy}^{AHE} (S/cm)	θ^{AHE}(%)
573	51.7	24.1	24.2	100	0	0	3.38	4061	285	7.1
673	51.8	22.8	25.4	11	89	0	3.67	6778	723	10.8
773	50.5	22.5	27.0	13	87	23	3.35	7766	905	11.8

concentration remained above 100 ppm. In contrast, the S parameters at 4–6 keV slightly decreased from $T_A = 573$ to 773 K, as highlighted by comparison with the broken lines in the lower two plots. This indicates that the divacancies were partially annealed out near the Co_2MnGa/MgO interface.

As shown by the XRD patterns, increasing the annealing temperature facilitated the crystal ordering from *A*2 to $L2_1$. This implies the occurrence of efficient atomic diffusion during annealing. Direct exchange between atoms in adjacent sublattices may require high energy. Hence, it is inferred that the divacancies assisted the atomic diffusion and consequently the development of the ordered structures. In this respect, prolongation of the annealing time beyond 3 h may prove effective for increasing the fraction of the $L2_1$ phase, although additional care should be taken to prevent the sublimation of Mn atoms.

C. Magnetic and electrical performance

Figure 5(a) presents the room-temperature M–H curves measured for the Co_2MnGa films after annealing. As seen from the inset, clear hysteresis loops were observed, suggesting ferromagnetic characteristics. The saturation magnetization values were determined to be 3.38, 3.67, and 3.35 μ_B/f.u. for $T_A = 573$, 673, and 773 K, while the coercivity values were 32, 25, and 38 Oe,

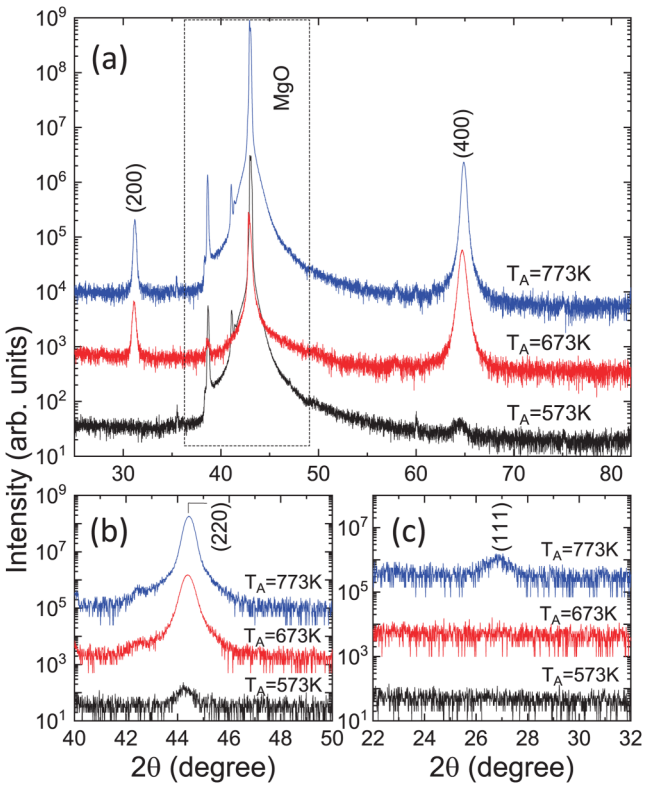

FIG. 2. XRD patterns acquired in the (a) out-of-plane scan mode and [(b) and (c)] tilted scan mode for Co_2MnGa films after annealing at 573, 673, and 773 K. (400) and (220) are fundamental reflections, while (200) and (111) are superlattice reflections indicating *B*2 and $L2_1$ structures, respectively.

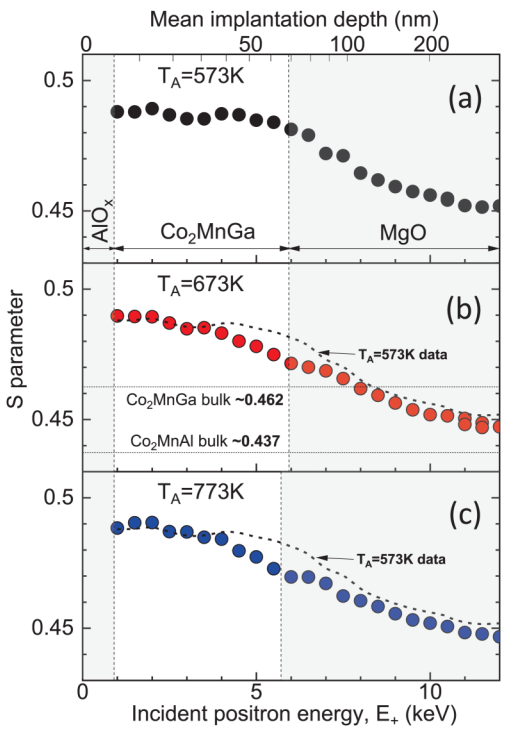

FIG. 3. (a)–(c) Positron annihilation S parameters as a function of incident positron energy (S–E curves) obtained for Co_2MnGa films after annealing at 573, 673, and 773 K. The errors of individual data are within the circles. The S parameters obtained for bulk Co_2MnGa and Co_2MnAl are indicated as horizontal lines in (b). In (b) and (c), the S–E curve for $T_A = 573$ K is plotted for comparison.

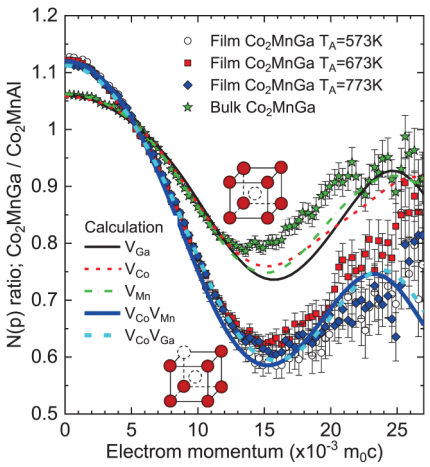

FIG. 4. DBAR spectra $N(p)/N_{ref}(p)$ obtained for Co_2MnGa films after annealing at 573 K (open circles), 673 K (closed squares), and 773 K (closed diamonds) and for a Co_2MnGa bulk single crystal (closed stars), where $N_{ref}(p)$ denotes the reference spectrum of Co_2MnAl. For better statistics, the spectra for the film and bulk samples were integrated at 1–4 and 15–20 keV, respectively. The thinner solid, dashed, and dotted-dashed curves denote the calculated spectra assuming Ga, Co, and Mn single vacancies, respectively. The thicker solid and dashed curves denote the calculated spectra assuming $V_{Co}V_{Mn}$ and $V_{Co}V_{Ga}$ divacancies, respectively. The configurations of single vacancy and divacancy are also schematically indicated.

respectively. The saturation magnetization value obtained for $T_A = 573$ K is below the ideal level for Co_2MnGa, namely, 3.7 μ_B/f.u. at room temperature.[33] This degradation is attributable to the overall crystal quality of the Co_2MnGa films, including the crystal disorder ($A2$ structure) and vacancy defects as discussed above. In fact, the saturation magnetization value of the $A2$ phase is reported to be significantly lower (2–2.5 μ_B) than that of the $B2$ phase.[34] The present film exhibited even better saturation magnetization value for the $A2$ phase, suggesting better quality as compared to that in the previous work. The dramatic degradation of saturation magnetization value in the $A2$ phase is also theoretically predicted for Co_2MnSi.[12,15] The saturation magnetization value obtained for $T_A = 673$ K (3.67 μ_B/f.u.) was comparable to the ideal value for the $L2_1$ phase. This is also reasonable since the saturation magnetization value for the $B2$ phase is reported to be only slightly lower than that of the $L2_1$ phase.[8,34]

However, the saturation magnetization value decreased at $T_A = 773$ K despite the further development of the $L2_1$ phase as revealed by the XRD measurements. This seems to be rather peculiar at first glance. Here, we focus on the depletion of Mn and Co (or conversely the enrichment of Ga) as seen in Table I. According to the theoretical study,[35] the saturation magnetization value is lost by 0.35 μ_B upon 10% Mn depletion (and instead 10% Ga enrichment), which is nearly the same as the present composition for $T_A = 773$ K. The degradation of magnetization from $T_A = 673$ to 773 K (3.67 to 3.35 μ_B/f.u.) is in excellent agreement with the above theoretical prediction. Consequently, it can be said that the $L2_1$ phase was developed at $T_A = 773$ K in the stoichiometric region,

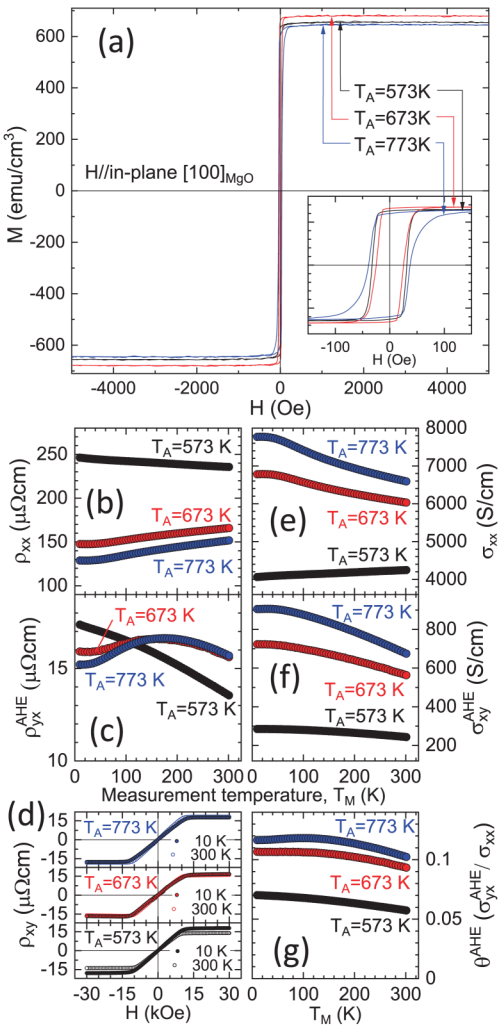

FIG. 5. (a) Room-temperature M–H curves under in-plane magnetization (the inset presents a magnified view to show the hysteresis), (b) longitudinal resistivities, (c) anomalous Hall resistivities, (e) longitudinal conductivities, (f) anomalous Hall conductivities, and (g) anomalous Hall angles as functions of temperature and (d) transverse resistivities as a function of magnetic field for Co_2MnGa films after annealing at 573, 673, and 773 K.

while the whole magnetization was lost due to the compositional unbalance between Mn and Ga.

Figures 5(b) and 5(e) show the longitudinal resistivities (ρ_{xx}) and conductivities (σ_{xx}), respectively, as a function of temperature measured for the Co_2MnGa films after annealing. It is seen that ρ_{xx} (σ_{xx}) for $T_A = 573$ K was the highest (lowest) among the three annealing conditions. Furthermore, the temperature dependences were indicative of somewhat semiconductor-like behavior. With increasing T_A, ρ_{xx} (σ_{xx}) decreased (increased) considerably and it displayed metallic temperature dependence.

Figure 5(d) shows the field dependences of transverse resistivities (ρ_{xy}). From this, the components related to the anomalous

Hall effect (saturation in a high field) were confirmed. By extrapolating the high-field resistivities to zero field, the anomalous Hall resistivities (ρ_{xy}^{AHE}) were obtained. Also, the anomalous Hall conductivities (σ_{xy}^{AHE}) were obtained by $\sigma_{xy}^{AHE} = \rho_{xy}^{AHE}/[(\rho_{xy}^{AHE})^2 + \rho_{xx}^2]$. Figures 5(c) and 5(f) show the temperature dependences of ρ_{xy}^{AHE} and σ_{xy}^{AHE}, respectively. Both ρ_{xy}^{AHE} and σ_{xy}^{AHE} for $T_A = 573$ K displayed monotonic temperature dependences as expected from the temperature dependence of ρ_{xx}. Although ρ_{xy}^{AHE} for $T_A = 673$ and 773 K increased from 10 to 100 K as expected from the temperature dependence of ρ_{xx}, it fell down above 200 K resulting broad peaks at 150–200 K. The reasons for the broad peaks are not clear at present moment, though one may speculate the effects of impurity, defects and alloying on the magnetic scattering of carriers. Contrarily, σ_{xy}^{AHE} exhibited monotonic temperature dependences likely corresponding to those for σ_{xx}. In the whole temperature range, σ_{xy}^{AHE} for $T_A = 773$ K exhibited the highest values. Figure 5(g) shows the anomalous Hall angles (θ^{AHE}) as a function of temperature. It was found that θ^{AHE} for $T_A = 773$ K reached 11.8% at 10 K. Thus, the post-growth annealing was effective for enhancing the anomalous Hall effect as well as the longitudinal transport properties. The maximum value of σ_{xy}^{AHE} was located in the region of the intrinsic anomalous Hall effect in the phase diagram of σ_{xy}^{AHE} vs σ_{xx} proposed theoretically.[36,37] Therefore, even in the present Co_2MnGa films with the $B2$ phase, the intrinsic mechanism ascribed to the characteristic Weyl semimetallicity dominates the anomalous Hall effect.

The improvement in the electrical transport properties with increasing annealing temperature may be associated with the development of the ordered structure and the partial disappearance of divacancies as discussed in Sec. III B. This implies that the further development of the $L2_1$ order and greater suppression of divacancies realize ideal performance. Increasing the annealing temperature and/or prolongation of the annealing time may be one approach. These will facilitate the development of the $L2_1$ order through atomic diffusion. In recent studies, fully $L2_1$-ordered Co_2MnGa films were successfully fabricated at higher deposition temperatures, i.e., 823–873 K.[6,8] The magnetizations were reported to be close to the ideal level. Although the obtained anomalous Hall angle and longitudinal conductivity were somewhat low,[8] the simultaneous enhancement of anomalous Hall angle and longitudinal conductivity seems to be feasible by changing the composition and hence the doping condition systematically.[6]

Nevertheless, we should recognize that the maximum value of σ_{xy}^{AHE} at low temperatures, approximately 900 S/cm, obtained for the films is still below the σ_{xy}^{AHE} observed for bulk Co_2MnGa (~2000 S/cm)[4] as well as the theoretical value of intrinsic anomalous Hall conductivity (~1600 S/cm).[2] Decomposing the temperature dependence of σ_{xy}^{AHE} indicated further degradation of the intrinsic term. Furthermore, σ_{xx} is less than half that for bulk Co_2MnGa ($\sim 2 \times 10^4$ S/cm). Ultimately, both the longitudinal and transverse transport properties were enhanced at $T_A = 773$ K but these improvements were still insufficient as compared to the bulk materials.

IV. CONCLUSION

We investigated the influence of post-growth annealing from $T_A = 573$ to 773 K on the properties of Co_2MnGa films. The obtained findings can be summarized as follows:

(i) Co_2MnGa could be epitaxially grown on MgO(001).
(ii) Mn sublimation started to occur at $T_A \geq 673$ K.
(iii) The crystal order changed from $A2$ to $B2$ plus $L2_1$ from $T_A = 573$ to 773 K.
(iv) The Co_2MnGa films contained divacancies at a concentration of at least 100 ppm, and these were partially annealed out at $T_A \geq 673$ K near the interface with MgO.
(v) The saturation magnetization was lower than the ideal value even at $T_A = 773$ K, where the $L2_1$ has been developed, probably due to the Mn depletion.
(vi) Both the longitudinal and anomalous Hall conductivities were dramatically enhanced from $T_A = 573$ to 773 K, although they remained much lower than ideal values.

Thus, the fabrication of highly ordered Co_2MnGa and the reduction of divacancies are thought to be crucial for realizing high electrical performance based on Weyl semimetallicity.

ACKNOWLEDGMENTS

This work was financially supported by a JSPS KAKENHI Grant-in-Aid for Scientific Research (S) (No. JP18H05246), a Grant-in-Aid for Scientific Research (A) (No. JP20H00299), and The Murata Science Foundation.

AUTHOR DECLARATIONS

Conflict of Interest

The authors have no conflicts to disclose.

DATA AVAILABILITY

The data that support the findings of this study are available within the article.

REFERENCES

[1]J. Kübler and C. Felser, Europhys. Lett. **114**, 47005 (2016).
[2]K. Manna, Y. Sun, L. Müchler, J. Kübler, and C. Felser, Nat. Rev. Matter. **3**, 244 (2018).
[3]I. Belopolski, K. Manna, D. S. Sanchez, G. Chang, B. Ernst, J. Yin, S. S. Zhang, T. Cochran, N. Shumiya, H. Zheng, B. Singh, G. Bian, D. Multer, M. Litskevich, X. Zhou, S. M. Huang, B. Wang, T. R. Chang, S. Y. Xu, A. Bansil, C. Felser, H. Lin, and M. Z. Hasan, Science **365**, 1278 (2019).
[4]A. Sakai, Y. P. Mizuta, A. A. Nugroho, R. Sihombing, T. Koretsune, M. Suzuki, N. Takemori, R. Ishii, D. Nishio-Hamane, R. Arita, P. Goswami, and S. Nakatsuji, Nat. Phys. **14**, 1119 (2018).
[5]S. N. Guin, K. Manna, J. Noky, S. J. Watzman, C. Fu, N. Kumar, W. Schnelle, C. Shekhar, Y. Sun, J. Gooth, and C. Felser, NPG Asia Mater. **11**, 16 (2019).
[6]K. Sumida, Y. Sakuraba, K. Masuda, T. Kono, M. Kakoki, K. Goto, W. Zhou, K. Miyamoto, Y. Miura, T. Okuda, and A. Kimura, Commun. Mater. **1**, 89 (2020).
[7]Q. Wang, Z. Wen, T. Kubota, T. Seki, and K. Takanashi, Appl. Phys. Lett. **115**, 252401 (2019).
[8]Z. Zhu, T. Higo, S. Nakatsuji, and Y. Ohtani, AIP Adv. **10**, 085020 (2020).
[9]M. P. Raphael, B. Ravel, Q. Huang, M. A. Willard, S. F. Cheng, B. N. Das, R. M. Stroud, K. M. Bussmann, J. H. Claassen, and V. G. Harris, Phys. Rev. B **66**, 104429 (2002).
[10]S. Picozzi, A. Continenza, and A. J. Freeman, Phys. Rev. B **69**, 094423 (2004).
[11]S. Picozzi and A. J. Freeman, J. Phys. Condens. Matter **19**, 315215 (2004).
[12]Y. Kota, H. Tsuchida, and A. Sakuma, J. Phys. Conf. Ser. **200**, 052012 (2009).

[13]B. Hülsen, M. Scheffler, and P. Kratzer, Phys. Rev. B **79**, 094407 (2009).
[14]J. Kudrnovský, V. Drchal, and I. Turek, Phys. Rev. B **88**, 014422 (2013).
[15]B. Pradines, R. Arras, I. Abdallah, N. Biziere, and L. Calmels, Phys. Rev. B **95**, 094425 (2017).
[16]V. Popescu, P. Kratzer, S. Wimmer, and H. Ebert, Phys. Rev. B **96**, 054443 (2017).
[17]M. Kogachi, S. Kikuchi, T. Fujiwara, and F. Hori, J. Alloys Compd. **480**, 462 (2009).
[18]K. Özdoğan, E. Sasioglu, and I. Galanakis, Phys. Stat. Sol. (PRL) **1**, 184 (2007).
[19]B. Pradines, R. Arras, and L. Calmels, J. Phys. Conf. Ser. **903**, 012030 (2016).
[20]R. Krause-Rehberg and H. S. Leipner, *Positron Annihilation in Semiconductors* (Springer, 1998).
[21]F. Tuomisto and I. Makkonen, Rev. Mod. Phys. **85**, 1583 (2013).
[22]K. Manna, L. Muechler, T. Kao, R. Stinshoff, Y. Zhang, J. Gooth, N. Kumar, G. Kreiner, K. Koepernik, R. Car, J. Kübler, G. H. Fecher, C. Shekhar, Y. Sun, and C. Felser, Phys. Rev. X **8**, 041045 (2018).
[23]T. Kono, M. Kakoki, T. Yoshikawa, X. Wang, K. Goto, T. Muro, R. Y. Umetsue, and A. Kimura, Phys. Rev. Lett. **125**, 216403 (2020).
[24]R. Y. Umetsu, K. Kobayashi, R. Kainuma, Y. Yamaguchi, K. Ohoyama, A. Sakuma, and K. Ishida, J. Alloys Compd. **499**, 1 (2010).
[25]X. Gonze, J.-M. Beuken, R. Caracas, F. Detraux, M. Fuchs, G.-M. Rignanese, L. Sindic, M. Verstraete, G. Zerah, F. Jollet, M. Torrent, A. Roy, M. Mikami, P. Ghosez, J.-Y. Raty, and D. Allan, Comput. Mater. Sci. **25**, 478 (2002).
[26]P. E. Blöchl, Phys. Rev. B **50**, 17953 (1994).
[27]J. P. Perdew, K. Burke, and M. Ernzerhof, Phys. Rev. Lett. **77**, 3865 (1996).
[28]P. J. Webster, J. Phys. Chem. Solids **32**, 1221 (1971).
[29]R. Y. Umetsu, K. Kobayashi, A. Fujita, R. Kainuma, and K. Ishida, J. Appl. Phys. **103**, 07D718 (2008).
[30]E. Boroński and R. M. Nieminen, Phys. Rev. B **34**, 3820 (1986).
[31]E. Clementi and C. Roetti, At. Data Nucl. Data Tables **14**, 177 (1974).
[32]Y. Takamura, R. Nakane, and S. Sugahara, J. Appl. Phys. **105**, 07B109 (2009).
[33]R. Y. Umetsu, K. Kobayashi, A. Fujita, R. Kainuma, K. Ishida, K. Fukamachi, and A. Sakuma, Phys. Rev. B **77**, 104422 (2008).
[34]Y. V. Kudryavtsev, V. A. Oksenenko, Y. P. Lee, Y. H. Hyun, J. B. Kim, J. S. Park, S. Y. Park, and J. Dubowik, Phys. Rev. B **76**, 024430 (2007).
[35]K. Özdoğan, E. Sasioglu, B. Aktas, and I. Galanakis, Phys. Rev. B **74**, 172412 (2006).
[36]S. Onoda, N. Sugimoto, and N. Nagaosa, Phys. Rev. Lett. **97**, 126602 (2006).
[37]S. Onoda, N. Sugimoto, and N. Nagaosa, Phys. Rev. B **77**, 165103 (2006).